



HAL
open science

High-Temperature Solar Methane Dissociation in a Multitubular Cavity-Type Reactor in the Temperature Range 1823–2073 K

Sylvain Rodat, Stéphane Abanades, Gilles Flamant

► **To cite this version:**

Sylvain Rodat, Stéphane Abanades, Gilles Flamant. High-Temperature Solar Methane Dissociation in a Multitubular Cavity-Type Reactor in the Temperature Range 1823–2073 K. *Sustainable Energy & Fuels*, 2009, 23 (5), pp.2666-2674. 10.1021/ef900037v . hal-02571379

HAL Id: hal-02571379

<https://hal.science/hal-02571379>

Submitted on 12 May 2020

HAL is a multi-disciplinary open access archive for the deposit and dissemination of scientific research documents, whether they are published or not. The documents may come from teaching and research institutions in France or abroad, or from public or private research centers.

L'archive ouverte pluridisciplinaire **HAL**, est destinée au dépôt et à la diffusion de documents scientifiques de niveau recherche, publiés ou non, émanant des établissements d'enseignement et de recherche français ou étrangers, des laboratoires publics ou privés.

High-temperature solar methane dissociation in a multi-tubular cavity-type reactor in the temperature range 1823-2073 K

*Sylvain RODAT**, *Stéphane ABANADES*, *Gilles FLAMANT*

Processes, Materials, and Solar Energy Laboratory, CNRS (PROMES-CNRS, UPR 8521), 7 Rue du
Four Solaire, 66120 Odeillo Font-Romeu, France

Abstract: Methane cracking is a possible route for the co-production of hydrogen and carbon black avoiding CO₂ emission. An indirect heating solar reactor prototype, allowing thermal dissociation of methane without catalyst, is tested at high temperatures. It is composed of a cubic graphite cavity receiver (20 cm side) equipped with four independent vertical tubular reaction zones. The concentrated solar radiation (2-4 MW/m²) is absorbed through an hemispherical quartz window by a 9 cm-diameter aperture. A set of experimental results on solar methane dissociation is presented for the temperature range 1823-2073 K. The effects of temperature, residence time from 10 ms and beyond 100 ms, gas flow-rates up to 12 NL/min (2×10^{-4} Nm³s⁻¹) of methane, and methane concentration up to 100% are investigated. Moreover, an experimental run was also carried out with natural gas instead of pure methane. Typical hydrogen and carbon mass balances show that methane is efficiently converted into hydrogen whereas it is not as well converted into solid carbon due to the production of acetylene. A two-step mechanism for methane dissociation is presented in order to define accurately the reactor efficiencies (thermal efficiency and solar-to-hydrogen thermo-chemical conversion).

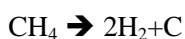
* Corresponding author. Fax: +33 4 68 30 29 40.

E-mail address: sylvain.rodatt@promes.cnrs.fr .

Keywords: Hydrogen production; Concentrated solar energy; Methane dissociation; Solar reactor; Natural gas; Carbon black.

1-Introduction

In order to counter the rising CO₂ emissions, the decarbonisation of energy is required and hydrogen appears as the most promising energy carrier. Natural gas (mainly composed of methane) may play a major role on the way toward a carbon free energy¹. It is the cleanest hydrocarbon fuel and it can benefit from transportation infrastructures. Nowadays, hydrogen is mainly produced from steam methane reforming², while carbon black is principally produced from the furnace process³. Both processes release large amounts of CO₂ in the atmosphere. Solar thermal methane cracking could be a solution for the clean co-production of hydrogen and carbon black. About 92% of the pollution associated with the two conventional processes is eliminated⁴. The overall reaction can be written as:



(1)

$$\Delta H^\circ = 75 \text{ kJ mol}^{-1} \text{ (216 kJ mol}^{-1} \text{ for CH}_4 \text{ at 298 K and products at 2000 K).}$$

The reaction is endothermic and solar thermal energy is used as power input, which results in the absence of CO₂ release in the process. At thermodynamic equilibrium, the dissociation is complete for temperatures beyond 1500 K⁵. Nevertheless, Holmen et al.⁶ point out the presence of products such as C₂H₆, C₂H₄, and C₂H₂ depending on the residence time. These species are the ones involved in the commonly accepted dehydrogenation of methane⁷. Thermodynamic equilibrium is not reached due to kinetic limitations. The overall decomposition of methane has been studied by investigating either a catalytic or a non-catalytic reaction. For non-catalytic reaction, activation energies range between 312 kJ/mol⁸ and 451 kJ/mol⁹, whereas activation energies are lower (143 kJ/mol¹⁰ - 236 kJ/mol¹¹) for the catalytic decomposition reaction.

In previous works on methane cracking, Lédé et al.¹² mentioned in 1978 the use of a solar reactor to apply thermal shocks to methane. A complete bibliographic survey on methane pyrolysis after 1960 was published by Billaud et al.¹³. Solar thermal cracking of methane also enabled the production of nanotubes¹⁴. Special interest was given to solar methane cracking for the co-production of hydrogen and

carbon black during the last five years. Two possible reactor designs were investigated, the direct¹⁵⁻¹⁹ and the indirect heating concepts^{2,4,20}. In the latter configuration, the solar irradiated zone is separated from the reacting flow whereas in the former, no separation is used, and particles seeding is required for efficient gas heating.

This work reports on the results obtained with a novel prototype-scale solar reactor (mean power: 20 kW) featuring a cubic graphite cavity (behaving as a black-body cavity) with four vertical inside tubular reaction zones. This design enables the control of the reactor tube temperature and is also suitable for scaling-up. Previous results on low temperature runs (in the range 1670-1770 K) have already been reported and have permitted to validate the Dsmoke kinetic code for the chemical reaction modelling applied to methane decomposition²¹. It also showed that increasing the temperature favour the methane conversion. Therefore, a second series of experiments at higher temperatures was performed in the range 1823-2073 K and the noteworthy results are discussed in the following sections.

2- Experimental Section

2.1-Design of the reactor

The reactor is presented in Fig. 1. It is composed of a graphite cavity receiver of cubic shape. Its side is 20 cm long and the aperture diameter is 9 cm. The reactor was designed for a nominal power in the range 15-25 kW. Inside the cavity, four independent and identical tubular reaction zones are positioned vertically and work in parallel. Each reaction zone is composed of two concentric tubes (Fig. 2). This design warrants a pre-heating of the feed gas by the hot products. The innermost tube is 4 mm i.d. and 12 mm o.d., while the outer tube is 18 mm i.d. and 24 mm o.d.. A mixture of methane and argon is fed in the innermost tube and the products flow out through the annular space between the two tubes. The total tube length is 380 mm: 178 mm are heated in the graphite cavity directly exposed to solar irradiation, while the remaining length goes through the insulating layers. Three different insulating

layers surround the graphite cavity in order to limit conduction losses. They form an insulation layer of 0.15 m thickness (0.05 m for each insulating material). The 3 insulating materials are a graphite felt in contact with the cavity ($\lambda=0.53 \text{ W}\cdot\text{m}^{-1}\cdot\text{K}^{-1}$ at 1873 K), an intermediate refractory ceramic fiber operating up to 1873 K (62% Al_2O_3 , 30% SiO_2 , $\lambda=0.35 \text{ W}\cdot\text{m}^{-1}\cdot\text{K}^{-1}$ at 1673 K), and an outer microporous insulator operating up to 1273 K (20% ZrO_2 , 77.5% SiO_2 , 2.5% CaO , $\lambda=0.044 \text{ W}\cdot\text{m}^{-1}\cdot\text{K}^{-1}$ at 1073 K). The reactor shell (535x535x373 mm) is made of stainless steel. As far as the front face is concerned, it is aluminum-made with water-cooling channels. A water-cooled copper-made component enables to hold the hemispherical quartz window. This transparent window closes the cavity, which helps to create an inert atmosphere. It prevents the graphite from oxidizing since the graphite cavity is swept by a nitrogen flow. Both the direct concentrated solar radiations from the sun and the IR radiations from the cavity walls contribute to the tubes heating. The solar concentrating system used is the 1 MW solar furnace of the CNRS-PROMES laboratory. It is composed of a field of 63 sun-tracking heliostats (45 m² each) and a parabolic concentrator (1830 m²) delivering up to 9000 suns at the focal point. For the experiments at 15-25 kW scale, only a limited number of heliostats (25) was used along with a shutter to control the incoming flux density in the range 2-4 MW/m². Then, the reactor aperture (9 cm-diameter) determined the absorbed solar power.

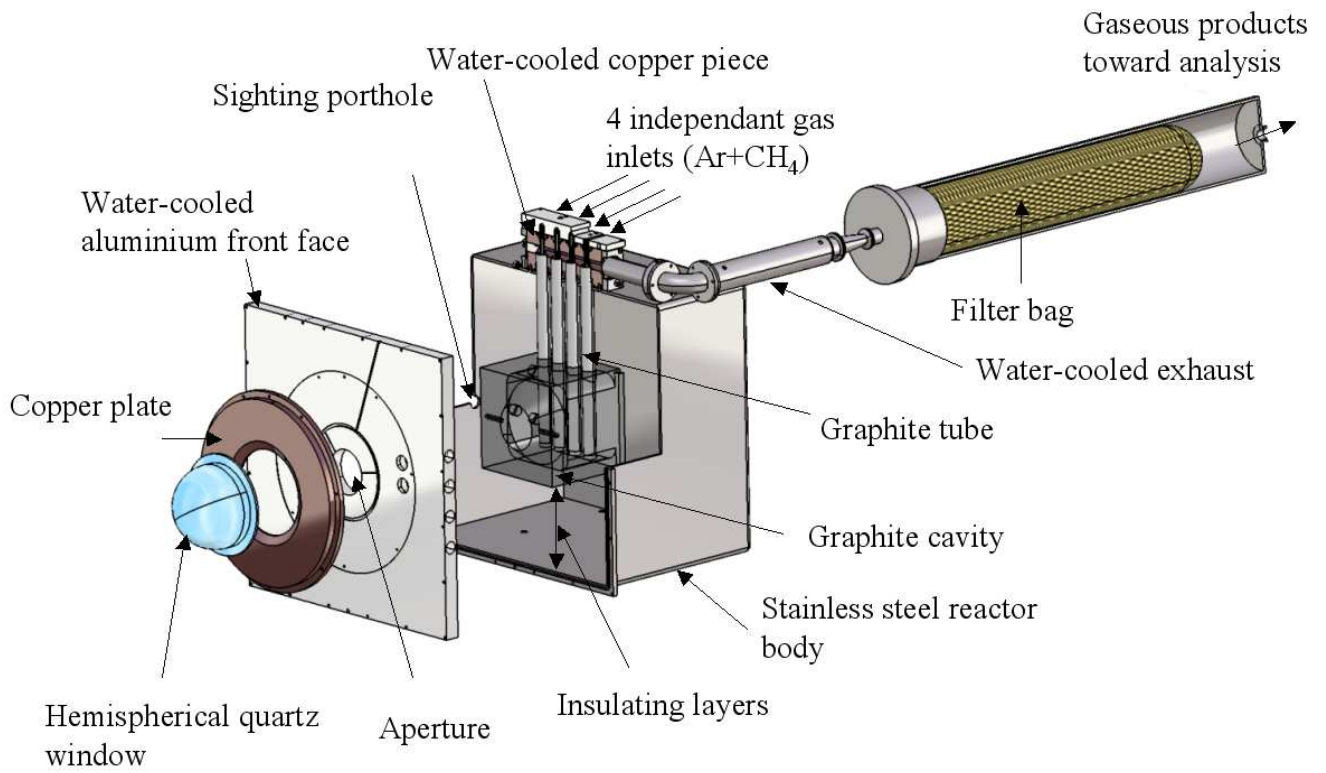


Figure 1. Scheme of the prototype-scale solar reactor and filter

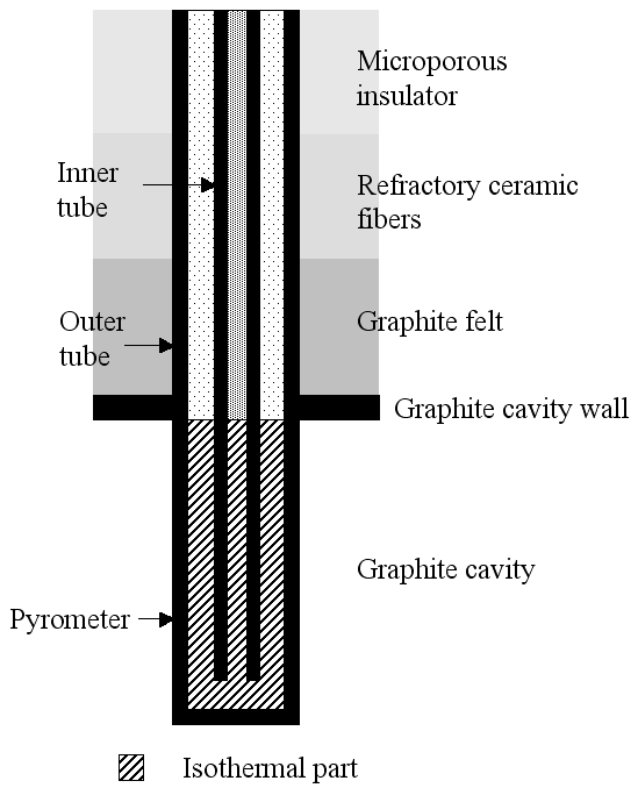


Figure 2. Scheme of the concentric tubes

2.2-Experimental procedure

Each experiment starts with a heating period (about 30 min) with an argon flow in the tubes in order to reach the targeted temperature. Temperature is controlled thanks to a solar-blind optical pyrometer (wavelength: 5.14 μm) pointing toward a tube wall through a CaF_2 window. A type B thermocouple (Pt–Rh) is placed in contact with the graphite cavity but has to be removed for temperatures above 1973 K (maximal working temperature for this device). Once the desired temperature is reached, a controlled mixture of argon and methane can be injected. This is enabled thanks to 8 mass-flow controllers (4 for methane and 4 for argon). Two mass-flow controllers are dedicated to each tube (Brooks Instruments model 5850 S, precision 0.7% of the measurement \pm 0.2% of the full scale, range 0-10 NL/min ($0-1.67 \times 10^{-4} \text{ Nm}^3 \text{ s}^{-1}$) for methane and 0-20 NL/min ($0-3.33 \times 10^{-4} \text{ Nm}^3 \text{ s}^{-1}$) for argon, where NL means Normal Liter that corresponds to one liter at normal conditions (101,325 Pa, 273.15 K)). There is no gas pre-heating before entering the reactor tubes since the gases are fed through a water-cooled copper component at the top of the reactor (Fig. 1). When leaving the reactor tubes, the gas products are collected in this same water-cooled copper component that allows the cooling of products below 373 K. Then, the gases flow in a water-cooled pipe before entering a solid-gas separation unit. Accordingly, the products flow through a filter bag (diameter: 127 mm, length: 800 mm) to separate carbon particles. It is made of Ryton with a Mikrotex membrane (type 3601-57, 500 g/m^2). Then, a bypass stream to be analyzed is aspirated through a set including a primary sampling pump that feeds a continuous analyzer and a secondary sampler (peristaltic pump) that feeds a gas chromatograph (GC, Varian CP 4900). The GC is equipped with 2 channels (the retention times are reported after each relevant species): channel 1 (MolSieve 5A PLOT 10M) for H_2 (25 s), CH_4 (41 s); channel 2 (PoraPLOT U 10M) for hydrocarbons such as CH_4 (22 s), C_2H_6 (43 s), C_2H_4 (37 s), C_2H_2 (54 s), and H_2 (21 s). The carrier gas used for chromatography analysis is argon, also used as buffer gas during methane cracking experiments, thereby eliminating the matrix effects. Continuous analysis of methane and hydrogen is enabled by a specifically

devoted multi-component gas analyser (Rosemount NGA 2000 MLT3, resolution: 1% of the full scale), and the methods used for H₂ and CH₄ analysis are thermal conductivity and non-dispersive infrared detections, respectively. The measurement of CH₄ concentration is used for interference cross-compensation in the measurement of H₂. The operation under reduced pressure (about 40 kPa) is enabled thanks to the use of a venturi vacuum pump (P6010 SI32-3X4, feed pressure 400 kPa, maximum vacuum flow of 3.2 NL/s ($5.33 \times 10^{-5} \text{ Nm}^3 \text{ s}^{-1}$) at -40 kPa). In order to monitor the pressure in each tube, absolute pressure transmitters with ceramic cells equip each tube entrance. The measurement scale is 0-400 kPa and the precision is +/- 0.30% of the full scale.

2.3-Experimental conditions

The investigated temperature range is 1823-2073 K. Temperature was proved to be homogeneous in the graphite cavity according to numerical simulations²². They also confirmed that the gas temperature has reached the wall temperature at the pyrometer position (Fig. 2). The methane mole fraction varies between 10% and 100% with a total methane flow-rate ranging between 0.8 NL/min and 12 NL/min (1.33×10^{-5} and $2 \times 10^{-4} \text{ Nm}^3 \text{ s}^{-1}$). The absolute pressure is about 40 kPa inside the tubes. The flow is laminar (Reynolds number < 2000). The typical mean duration of an experimental run at a given temperature is 45 min before tube blocking (due to carbon accumulation), and it depends strongly on the experimental conditions (dilution ratio, methane flow-rate and conversion). The pre-heating period is about half an hour.

3-Results and Discussion

For each experimental condition, various parameters are calculated:

- The residence time τ of the gas species is calculated by dividing the volume of the isothermal part of the tube (part inserted in the graphite cavity, Fig. 2) by the volumetric inlet flow-rate of

argon and methane at the real tube temperature and pressure. It is often referred as “space time”²³. It permits to give a characteristic reaction time even if chemical expansion is not included. In the following discussion, “residence time” will always refer to this definition.

$$\tau = \frac{V_r}{Q_0} \quad (2)$$

- The CH₄ conversion gives the proportion of methane that has been transformed and it is defined as:

$$X_{CH_4} = \frac{F_{0,CH_4} - F \cdot y_{CH_4}}{F_{0,CH_4}} \quad (3)$$

- The H₂ yield is the proportion of methane that has been converted into hydrogen and it is calculated from:

$$Y_{H_2} = \frac{F \cdot y_{H_2}}{2 \cdot F_{0,CH_4}} \quad (4)$$

- The C yield is the proportion of methane that has been converted into solid carbon and it is expressed as:

$$Y_C = \frac{F_{0,CH_4} - (F \cdot y_{CH_4} + 2 \cdot F \cdot y_{C_2H_2} + 2 \cdot F \cdot y_{C_2H_4} + 2 \cdot F \cdot y_{C_2H_6})}{F_{0,CH_4}} \quad (5)$$

where F_{0,CH_4} is the inlet molar flow-rate of CH₄, y_i is the mole fraction of species i , and F is the total outlet flow-rate (including argon as buffer gas) obtained from:

$$F = F_{Ar} + F \cdot y_{CH_4} + F \cdot y_{H_2} + F \cdot y_{C_2H_2} + F \cdot y_{C_2H_4} + F \cdot y_{C_2H_6} \quad (6)$$

F_{Ar} is the molar flow-rate of Ar.

- The reactor thermo-chemical efficiency represents the fraction of solar energy that is converted and stored in a chemical form as hydrogen¹⁸:

$$\eta_{ch} = \frac{F_{0,CH_4} \cdot X_{CH_4} \cdot \Delta H_{\text{Reactants}(T_0) \rightarrow \text{Products}(T_{\text{reactor}})}}{P_{\text{solar}}} \quad (7)$$

- The reactor thermal efficiency also takes into account the heating enthalpy of both the non-converted reactants and the inert gas, it is expressed as:

$$\eta_{th} = \frac{F_{0,CH_4} \cdot (1 - X_{CH_4}) \cdot \int_{T_0}^{T_{reactor}} C_{p_{CH_4}} \cdot dT + F_{0,CH_4} \cdot X_{CH_4} \cdot \Delta H_{Reactants(T_0) \rightarrow Products(T_{reactor})} + F_{Ar} \cdot \int_{T_0}^{T_{reactor}} C_{p_{Ar}} \cdot dT}{P_{solar}} \quad (8)$$

where ΔH ($J \cdot mol^{-1}$) is the enthalpy change of the reaction (1) when the reactants are fed at $T_0=298$ K and the products are obtained at $T_{reactor}$, P_{solar} is the solar power input (W), C_{p_i} is the specific heat of species i ($J \cdot mol^{-1} \cdot K^{-1}$, function of temperature).

This set of indicators is the foundation of the discussion below.

3.1-Steady state, stability, reproducibility

CH_4 and H_2 off-gas mole fractions given by the on-line analyzer are plotted in Fig. 3, along with the temperature measured by the pyrometer. Four consecutive experimental conditions are represented: the first run is carried out with 36 NL/min ($6 \times 10^{-4} \text{ Nm}^3 \text{ s}^{-1}$) of Ar and 8 NL/min ($1.33 \times 10^{-4} \text{ Nm}^3 \text{ s}^{-1}$) of CH_4 , the second run with 36 NL/min ($6 \times 10^{-4} \text{ Nm}^3 \text{ s}^{-1}$) of Ar and 12 NL/min ($2 \times 10^{-4} \text{ Nm}^3 \text{ s}^{-1}$) of CH_4 , the third run is identical to the first in order to test reproducibility, the last run is carried out with 28 NL/min ($4.67 \times 10^{-4} \text{ Nm}^3 \text{ s}^{-1}$) of Ar and 8 NL/min ($1.33 \times 10^{-4} \text{ Nm}^3 \text{ s}^{-1}$) of CH_4 .

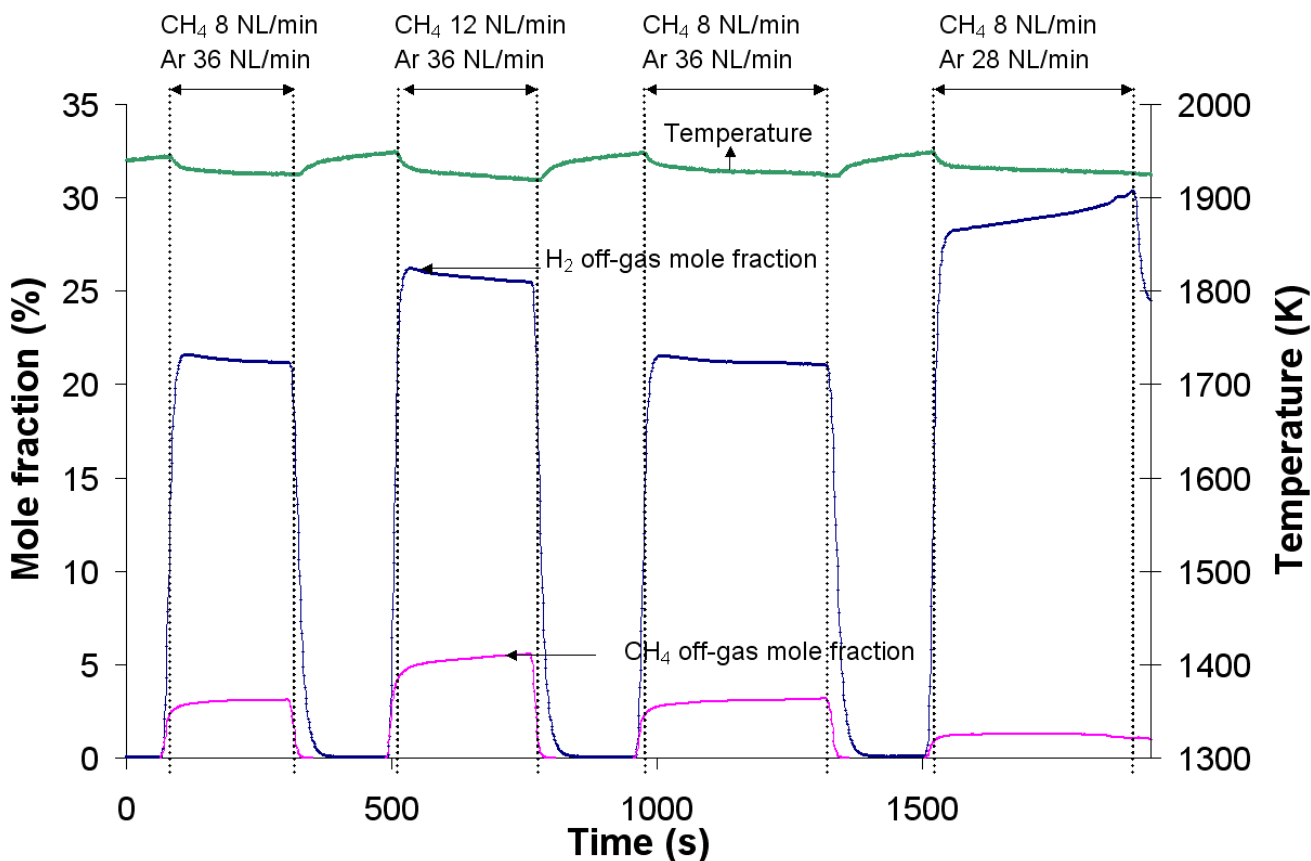


Figure 3. On-line H₂ and CH₄ off-gas mole fractions and temperature versus time for four consecutive runs

First, a plateau on the H₂ off-gas mole fraction is obtained for the first three experimental conditions after about 1 to 2 minutes. It shows that steady state is rapidly reached. For the last experimental condition, this plateau is not observed even after 6 min. and the H₂ mole fraction increases with time. This is due to a pressure increase in the reactor tubes as a result of tube blocking by carbon deposition. Consequently, the residence time increases and so does the H₂ yield. The pressure can increase from 40 kPa to 100 kPa in a few minutes, consequently the experiment is stopped.

Then, the first and third experimental runs prove that the same results are achieved for the same experimental conditions, both for H₂ and CH₄ off-gas concentrations (less than 1% difference on the CH₄ conversion and H₂ yield); and that there is no influence of the previous experimental conditions.

Finally, the temperature measurement shows fluctuations depending on the presence or absence of methane in the flow. As soon as methane is injected, the temperature decreases whereas it increases

when stopping the methane flow (argon flow-rate is maintained). The variation is about 20-30 K. The decrease of temperature when CH₄ is injected stems from the endothermic dissociation reaction. Thus, a slight reactor over-heating was set under argon flow before CH₄ injection to anticipate the temperature decrease and to reach the given reaction temperature during experiments.

3.2-Temperature influence

A maximum working temperature of 2073 K has been achieved. In Fig. 4, CH₄ conversion and C₂H₂ mole fraction are plotted versus residence time for different temperatures (1823 K, 1973 K, and 2073 K). The methane mole fraction in the inlet gas is kept constant at 20%. The total gas flow-rate is changed, which thereby determines the gas residence time. The influence of temperature is clear: the higher the temperature, the higher the conversion for a given residence time. For a 11 ms residence time, CH₄ conversion is 79%, 93%, and 100% at 1823 K, 1973 K, and 2073 K, respectively. The methane conversion is total for temperatures higher than 1823 K and residence times longer than 25 ms. Concerning C₂H₂ mole fraction in the off-gas, it seems to be more affected by residence time than by temperature. The lowest C₂H₂ concentrations are reached for the highest residence times.

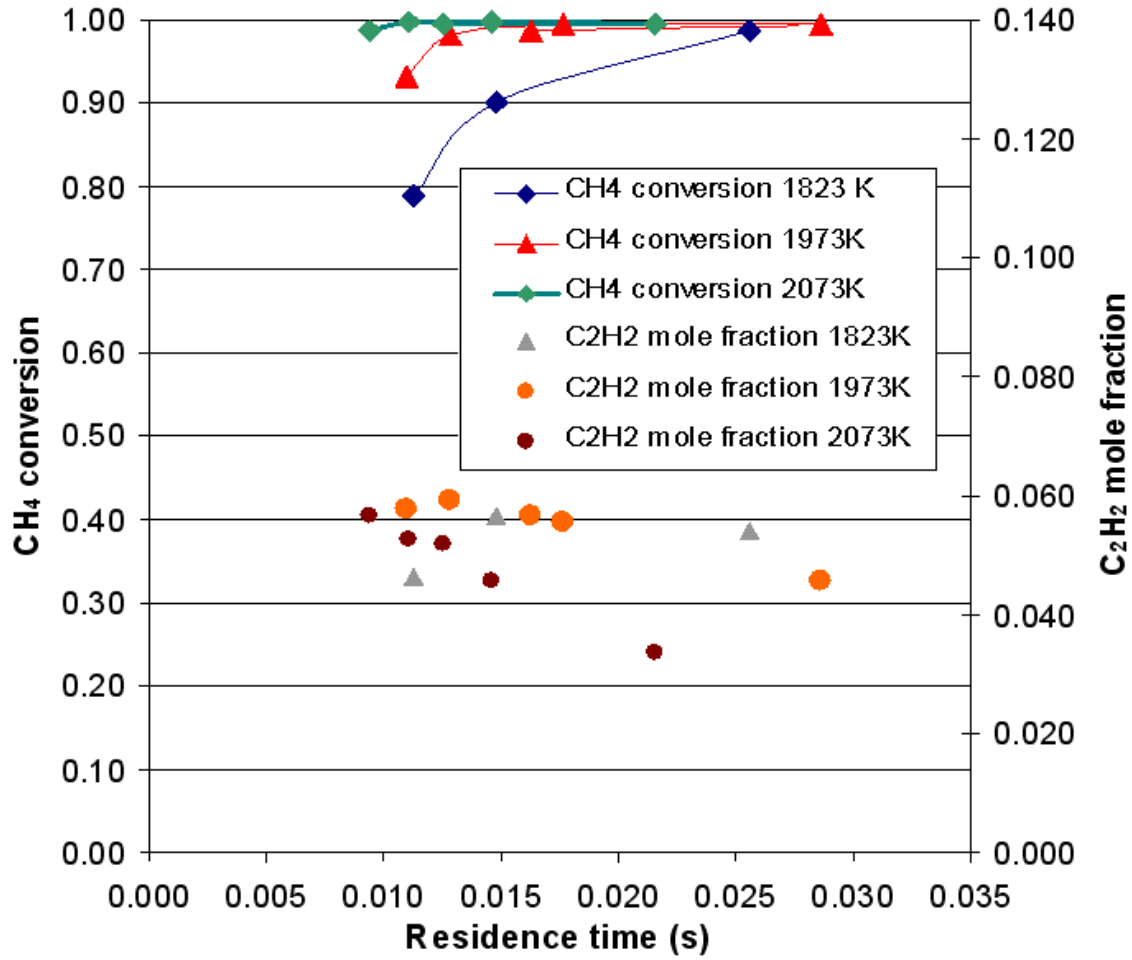


Figure 4. Temperature dependence of CH₄ conversion and C₂H₂ off-gas mole fraction versus residence time (CH₄ mole fraction in the feed: 20%)

Assuming a first order kinetic expression¹⁶ and an ideal plug-flow reactor model, the residence time τ can be calculated from¹⁹:

$$k\tau = -(1+\alpha)\beta \ln(1-X_{CH_4}) - \alpha\beta X_{CH_4} \quad (9)$$

where α is the chemical expansion factor, β is the physical dilatation factor, and k is the kinetic rate constant, following an Arrhenius law:

$$k = k_0 \cdot \exp(-E_a/RT) \quad (10)$$

where E_a denotes the activation energy (J/mol), k_0 the pre-exponential factor (s^{-1}), R the universal gas constant (8.314 J/mol K), and T the absolute temperature (K).

Thus, it is possible to determine the kinetic rate k for different experimental temperatures. Data from previous reported results at lower temperatures²¹ are also included. Then, from the plot $\ln(k)=f(1/T)$, a linear regression (determination factor = 0.9982) allows estimating a pre-exponential factor of $1.42 \times 10^7 s^{-1}$ and an activation energy of 172 kJ/mol. These values are consistent with previously reported activation energy for heterogeneous (catalytic) methane decomposition. The produced carbon black can play the role of catalyst¹¹. This simplified model permits to estimate that the incertitude (for $T=1823$ K) on CH_4 conversion is $\pm 1\%$ for a temperature incertitude of ± 10 K (that corresponds to the incertitude of experimental temperature measurements). Similarly, the incertitude on CH_4 conversion is less than $\pm 2\%$ if the residence time is estimated at $\pm 10\%$. A variation of $\pm 6\%$ of the activation energy (estimated incertitude of the slope) also affects the CH_4 conversion by $\pm 17\%$. Thus, uncertainties on the temperature or the residence time have a weak influence on the CH_4 conversion, whereas the value of the activation energy is more critical and it just provides an order of magnitude of the kinetic parameters.

3.3-Residence time influence

The influence of residence time was studied at a given temperature for a constant CH_4 mole fraction in the feed gas mixture (10%). Residence times between 15 ms and 70 ms were tested at 1823 K (Fig. 5). For clarity reasons, C_2H_4 mole fraction is not represented because it was always below 400 ppm. C_2H_6 was not detected.

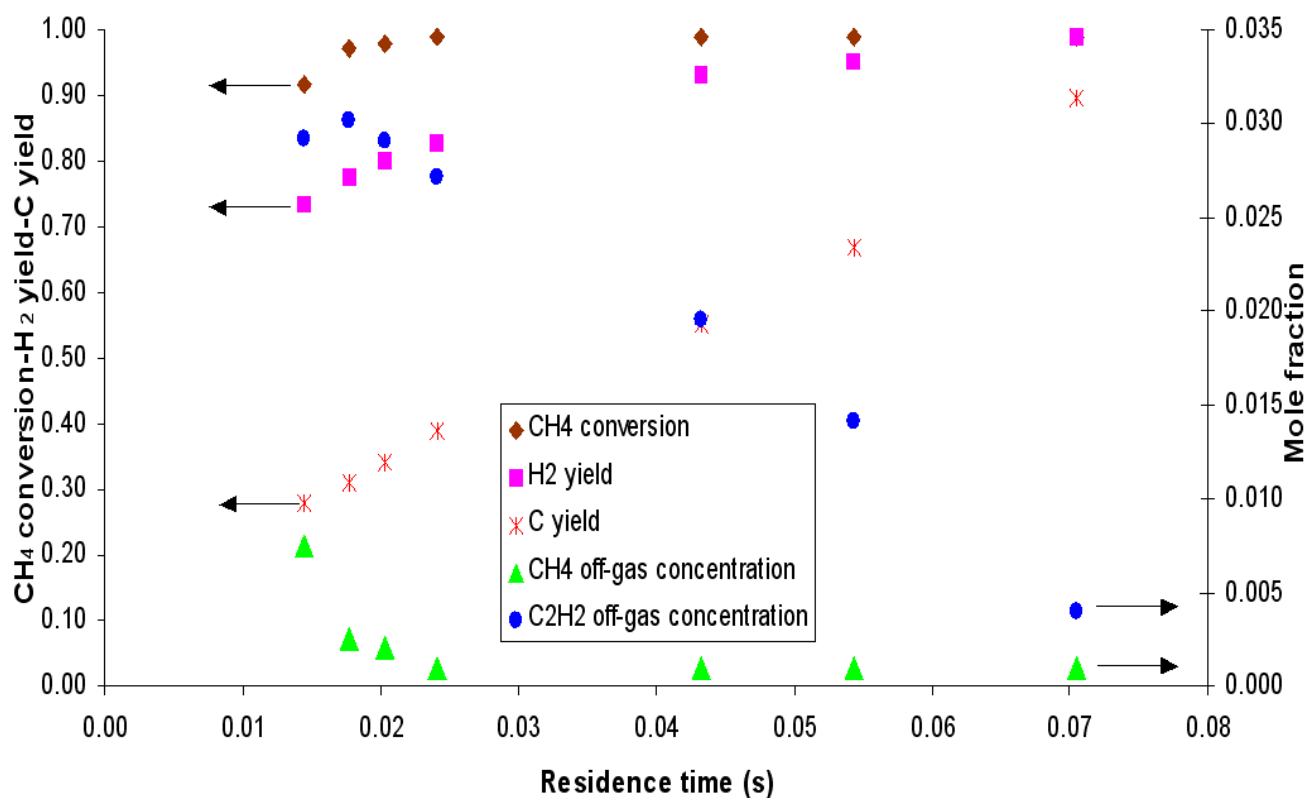


Figure 5. CH₄ conversion, H₂ yield, C yield, CH₄ and C₂H₂ off-gas mole fractions versus residence time (T = 1823 K, CH₄ mole fraction in the feed: 10%)

In order to change the residence time, flow rates were modified. The first conclusion is that the CH₄ conversion and the H₂ yield are improved when increasing the residence time. A more in-depth analysis of the results also gives a scheme of the methane decomposition sequence. For residence times between 15 ms and 18 ms, the H₂ yield increases due to a better CH₄ decomposition rate (off-gas concentration of CH₄ decreases), while the off-gas concentration of C₂H₂ slightly increases. It means that methane is first converted into acetylene ($2\text{CH}_4 \rightarrow \text{C}_2\text{H}_2 + 3\text{H}_2$), thus releasing 1.5 mole of H₂ per mole of CH₄ converted. For longer residence times, the H₂ yield is enhanced due to acetylene decomposition. Similar trends are observed in Fig. 4. For the lowest temperature (1823 K), C₂H₂ off-gas concentration presents a maximum whereas it decreases quite monotonically for higher temperatures because the maximum may occur at shorter residence times. This suggests that the rate of C₂H₂ formation becomes lower than the rate of C₂H₂ decomposition at any temperatures. Acetylene constitutes a reaction intermediate as

reported previously²⁴. Carbon yield is also represented and it can be observed that the decrease in the C₂H₂ off-gas concentration corresponds to an increase in carbon yield. C₂H₂ is thus converted into carbon black and H₂. A residence time of 70 ms is needed in order to reach an off-gas C₂H₂ mole fraction lower than 0.5%. A methane mole fraction of 50% in the feed gas mixture was also experimented at 1923 K for a residence time of 79 ms, and the resulting off-gas C₂H₂ mole fraction was less than 300 ppm. With pure methane in the feed (without any argon flow), a residence time of 124 ms at 1923 K was reached and the off-gas C₂H₂ mole fraction was below 400 ppm. To increase hydrogen yield and avoid acetylene formation, long contact times are required, whereas very high temperatures are not favourable²⁵.

Instead of speaking in terms of space time based on the inlet gas flow-rate ($\tau = V_r/Q_0$), it would be possible to calculate the mean residence time that takes into account the flow-rate at the exit of the reactor:

$$\tau_m = \frac{V_r}{Q_0 \beta (1 + X_{CH_4} \alpha)} \quad (11)$$

If the reference is taken at the entrance of the isothermal part of the reactor where the reaction occurs, then $\beta=1$. Thus, $\tau = 1.10 \cdot \tau_m$ for a 10% CH₄ mole fraction in the feed ($\alpha = 0.1$) and $X_{CH_4}=1$. The “real” residence time (time required for an inert tracer to cross the reactor volume) is thus between the space time and the mean residence time. For sufficient dilution with argon, simulation results²¹ confirm that there is no significant difference between the “real” residence time and the space time. Obviously, the space time must be twice the mean residence time when complete dissociation is reached for pure methane. For this study on the influence of the residence time, a CH₄ mole fraction of 10% is low enough to assimilate the space time to the real residence time.

3.4-Influence of the CH₄ mole fraction in the feed

The influence of the methane concentration was investigated with a constant flow-rate of argon (18 NL/min, $3 \times 10^{-4} \text{ Nm}^3 \text{ s}^{-1}$) and a methane flow-rate varying from 2 NL/min to 10 NL/min (3.33×10^{-5} – $1.67 \times 10^{-4} \text{ Nm}^3 \text{ s}^{-1}$), that is to say, a methane mole fraction in the feed varying from 10% to 36% (Fig. 6). The corresponding residence times, calculated at the actual tube temperature (1923 K) and pressure of each experimental condition, varies from 20 ms to 17 ms. Thus, the residence is almost constant. Both CH_4 conversion and H_2 yield are plotted. The CH_4 conversion is actually declining when increasing CH_4 mole fraction in the feed. This may be due to the endothermic reaction. The H_2 yield seems to dwindle sooner. Then, the higher the CH_4 mole fraction in the feed gas, the higher the amount of H_2 produced, but the lower the CH_4 conversion. Nevertheless, 93% CH_4 conversion and 74% H_2 yield are still reached for a CH_4 mole fraction of 36% in the feed. Consequently, increasing the CH_4 mole fraction in the feed gas up to 36% allows enhancing the thermo-chemical efficiency, because a fairly good chemical conversion is maintained. An additional experimental run was also carried out at 1923 K for 100% methane in the feed. The dissociation was complete: the outlet H_2 flow-rate was twice the inlet CH_4 flow-rate. The residence time was 62 ms for 4 NL/min ($6.67 \times 10^{-5} \text{ Nm}^3 \text{ s}^{-1}$) of CH_4 (mean residence time from Eq. 11 of 31 ms). The quantity of by-products was negligible. Therefore, this run shows that reaction completion can be achieved with pure methane in the feed for a residence time much longer than the one used in Fig. 6. Nevertheless, one must point out that the long residence time due to the low gas velocity caused a substantial carbon deposit in the tubes. Even if increasing the mole fraction improves the efficiency of the reactor, high methane concentrations along with high residence times favor carbon deposition.

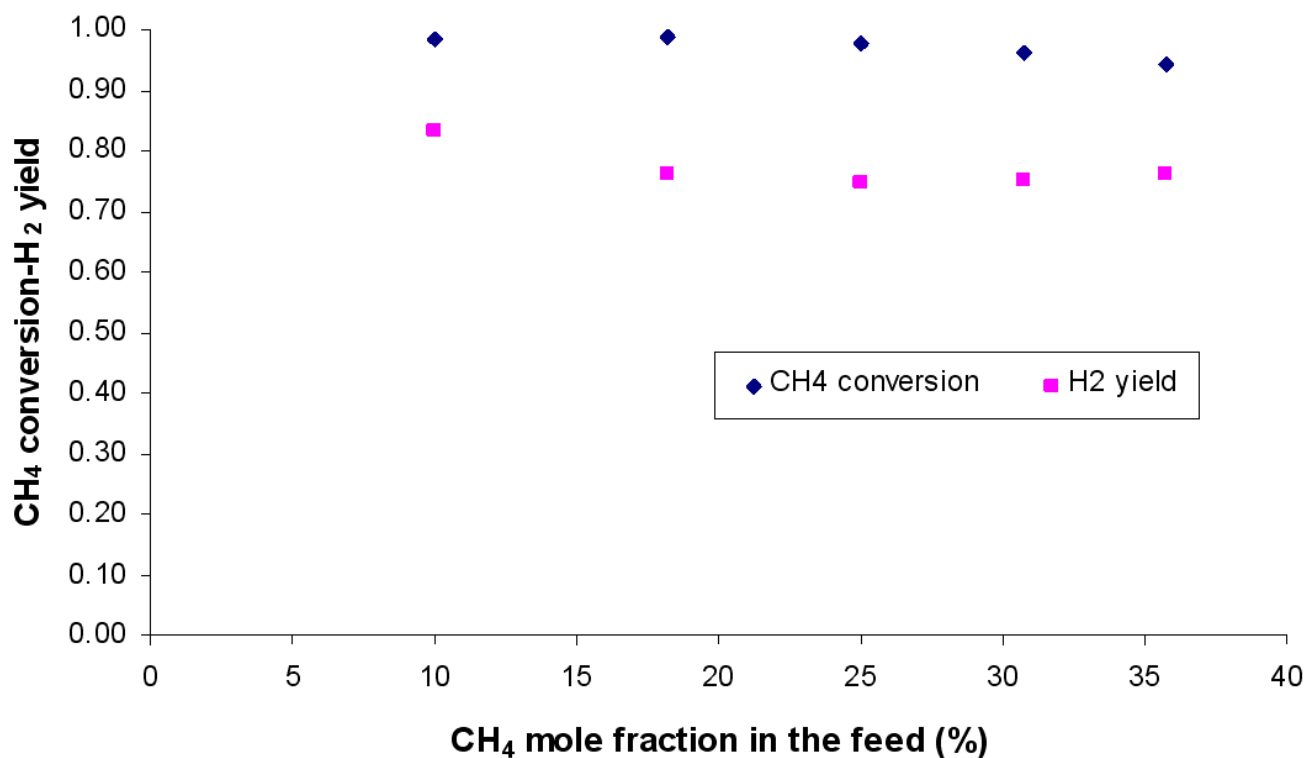


Figure 6. CH₄ conversion and H₂ yield versus CH₄ mole fraction in the feed at 1923 K

3.5-Methane cracking versus natural gas cracking

Natural gas was introduced instead of methane to examine the effect of feedstock composition. A chromatography analysis of this natural gas highlights the presence of about 9.5 % ethane and trace amounts of CO₂ and N₂. Fig. 7 plots the mole fractions of H₂, C₂H₂, and CH₄ as a function of residence time for methane cracking and natural gas cracking experiments at 1873 K. The comparison shows a small discrepancy limited to a few percents, which is in the range of experimental uncertainties. As predicted by the Dsmoke kinetic software²¹, there is no difference between natural gas cracking and pure methane cracking for a residence time higher than 1 ms. The only difference is expected for shorter residence times due to the presence of ethane (C₂H₆) that is easier to decompose than CH₄.

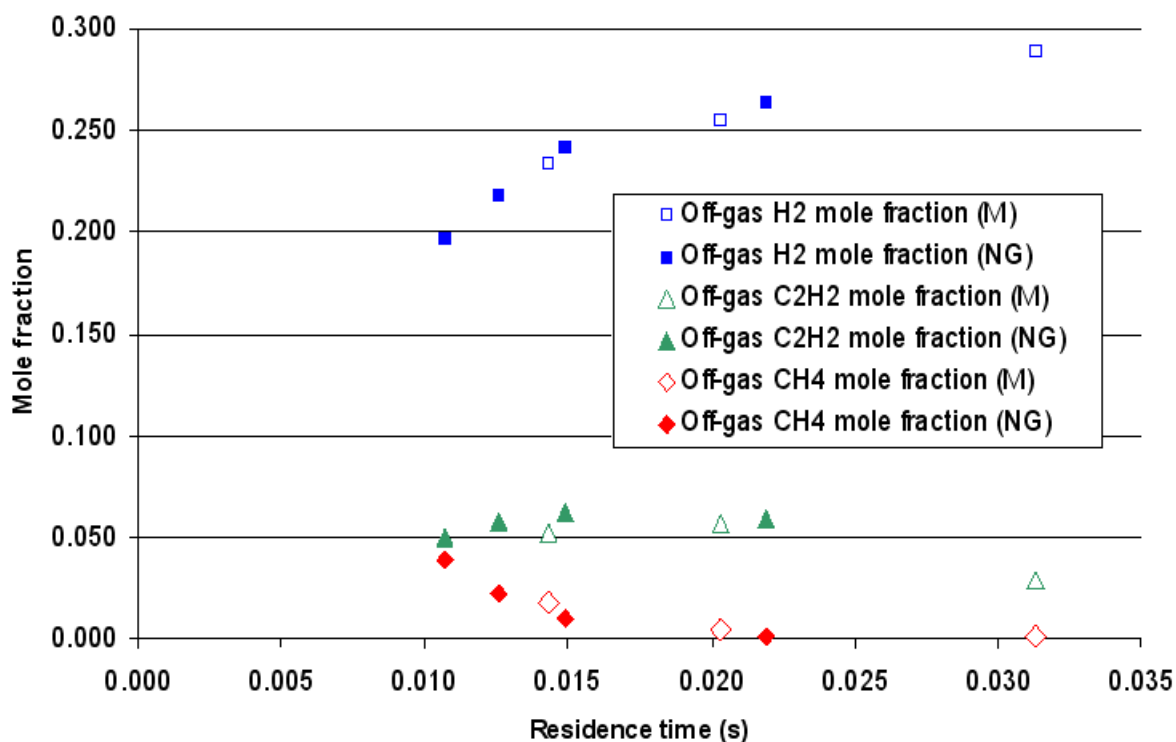


Figure 7. Off-gas H₂, C₂H₂, and CH₄ mole fractions for methane cracking (M) and natural gas cracking (NG) (T = 1873 K)

3.6-Carbon and hydrogen mass balances

A mass balance was established based on a series of 5 experimental runs at 1923 K with a constant argon flow-rate of 18 NL/min ($3 \times 10^{-4} \text{ Nm}^3 \text{ s}^{-1}$) and a methane flow-rate varying from 2 NL/min to 10 NL/min ($3.33 \times 10^{-5} - 1.67 \times 10^{-4} \text{ Nm}^3 \text{ s}^{-1}$). Fig. 8 plots the off-gas mole fractions of H₂, CH₄, and C₂H₂ throughout the experiment. The mass balances are obtained by integrating these data.

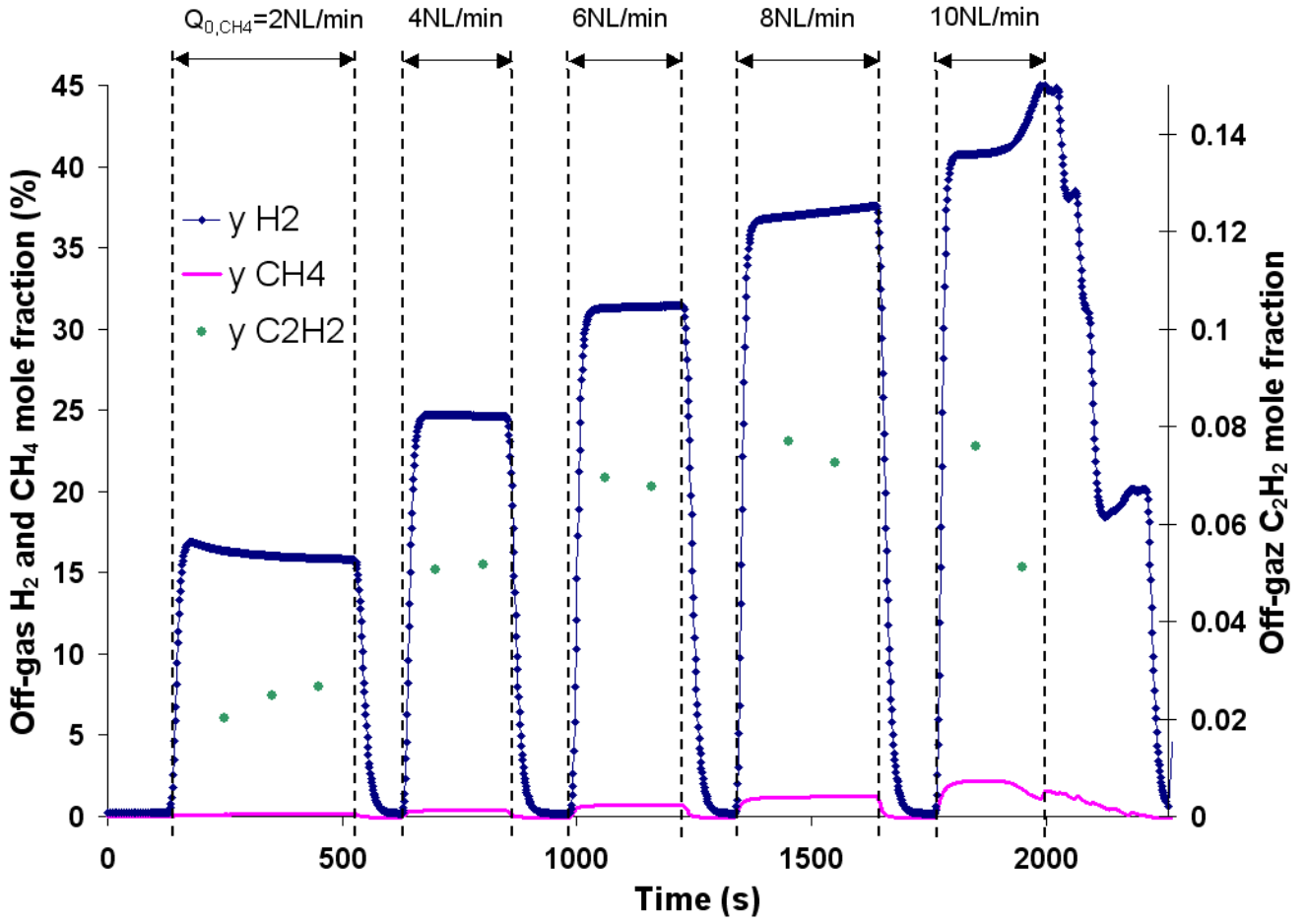


Figure 8. H₂, CH₄, and C₂H₂ mole fractions in the off-gas versus time (T = 1923 K, Ar flow-rate: 18 NL/min)

The reactor tubes and the filter were weighted before and after experiments. The mass of carbon accumulated in the tubes was 26.4 g, while 1.5 g of carbon was recovered in the filter. A total of 146.5 NL (0.1465 Nm³) of methane was introduced in the reactor. Then, a mass balance between the recovered solid carbon and the amounts of gaseous species in the off-gas shows that 93% of the initial carbon mass and 92% of the initial hydrogen mass are retrieved at the exit according to the following calculations (only H₂, C, CH₄, and C₂H₂ are taken into account, the other hydrocarbons are neglected):

$$C(\text{ratio}) = \frac{\frac{m_{CH_4}}{M_{CH_4}} + \frac{2m_{C_2H_2}}{M_{C_2H_2}} + \frac{m_C}{M_C}}{\frac{m_{0,CH_4}}{M_{0,CH_4}}} \quad (12)$$

$$H(\text{ratio}) = \frac{\frac{4m_{CH_4}}{M_{CH_4}} + \frac{2m_{C_2H_2}}{M_{C_2H_2}} + \frac{2m_{H_2}}{M_{H_2}}}{\frac{4m_{0,CH_4}}{M_{0,CH_4}}} \quad (13)$$

Fig. 9 shows the H mass balance. 75% of H atoms is found as H₂ gas, 14% is in the form of C₂H₂, 3% is contained in the unconverted CH₄, and the remaining 8% is thus attributed to other hydrocarbons. A fraction of the missing H-content may also be found in the carbon black although the H-content in the channel black (that presents the largest amount of hydrogen) is less than 1% (molar)³. According to this balance, CH₄ is efficiently converted into H₂ (75% H₂ yield).

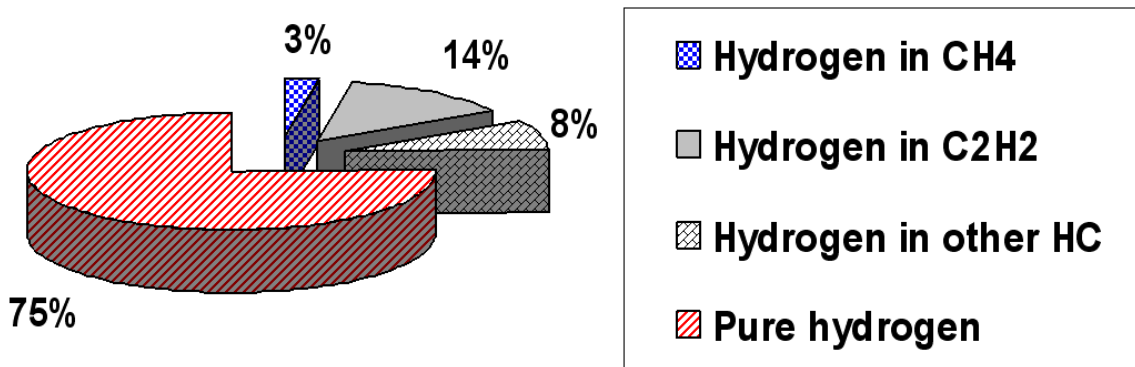


Figure 9. Typical H balance (T = 1923 K, Ar flow-rate: 18 NL/min)

Fig. 10 shows the C mass balance. 54 % of the carbon is contained in C₂H₂. Only 36% of the carbon is recovered as solid carbon either in the reactor tubes (34%) or in the filter (2%). 3% of carbon stays in the unconverted CH₄. The remaining part (7%) may be contained in other hydrocarbons or may correspond to un-removed solid carbon. Methane is not as well converted into solid carbon as it is in H₂ due to the substantial presence of C₂H₂.

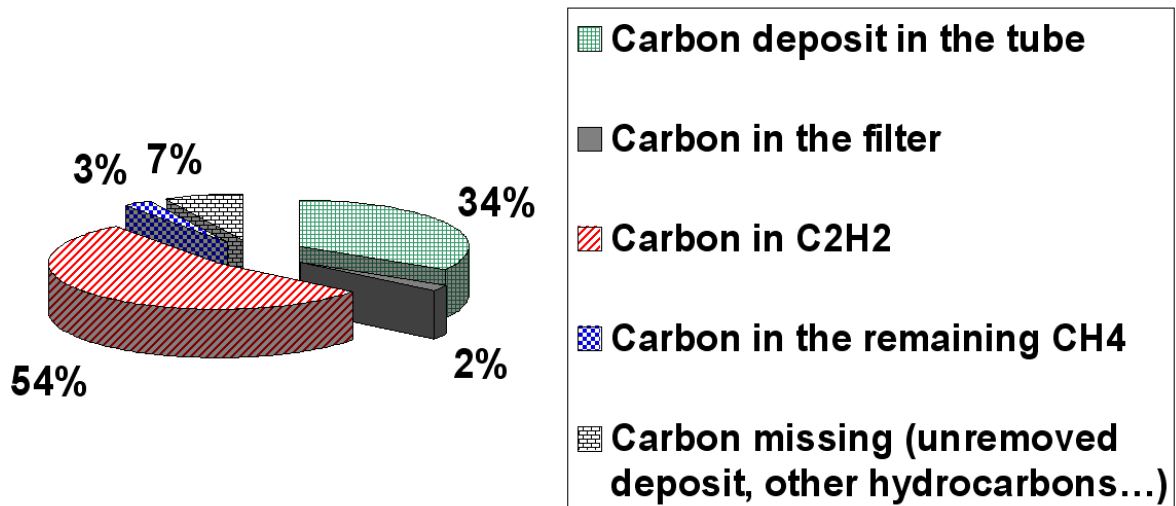
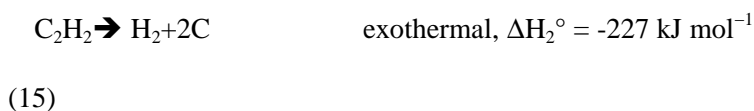
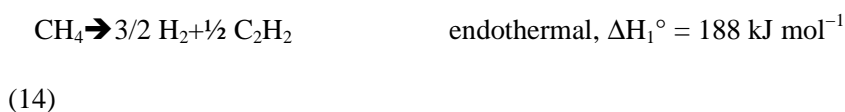


Figure 10. Typical C balance (T = 1923 K, Ar flow-rate: 18 NL/min)

3.7- Efficiency of the reactor

Owing to the production of by-products, the thermo-chemical efficiency as defined previously in Eq. (7) is not perfectly suitable. Indeed, it only gives the real efficiency of the reactor if the dissociation was complete, otherwise it is under-estimated. According to previous kinetic analyses of the reaction with a detailed chemical mechanism model, C₂H₆ and C₂H₄ are rapidly decomposed, and C₂H₂ is the only by-product present in appreciable amount at the exit of the reactor²¹, which is consistent with the gas analysis results. Thus, a two-step dissociation scheme is proposed according to the experimental results:



The standard enthalpy of methane-to-acetylene formation (Eq. 14) is more than twice the standard enthalpy of single-step methane dissociation (Eq. 1). In addition, a part of acetylene formed from methane is not dissociated into hydrogen, as shown by the analysis of the exhaust gas stream. This intermediate step involving acetylene must be taken into account in the calculation of the reactor

efficiency. The fractional conversions of the successive reactions (14) and (15) are the solutions of the following system:

$$F_{H_2} = (1/2 \cdot X \cdot Y + 3/2 \cdot X) \cdot F_{0,CH_4} \quad (16)$$

$$F_{C_2H_2} = (1 - Y) 1/2 \cdot X \cdot F_{0,CH_4} \quad (17)$$

where Y is the fractional conversion of reaction (15) defined as $Y = F_{H_2} / F_{0,C_2H_2}$ where F_{0,C_2H_2} is the molar flow-rate of acetylene issued from reaction (14). The fractional conversion X of reaction (14) should be equal to the CH_4 conversion X_{CH_4} defined in Eq. (3) if the real chemical mechanism was only composed of reactions (14) and (15). Nevertheless, this assumption is not exactly satisfied since X is always smaller (about 6%) than X_{CH_4} . This proves that the chemical mechanism includes additional steps and intermediates²⁶⁻²⁸. However, this two-step reaction model can fairly describe the production of the three major species (C, C_2H_2 , and H_2) in a simple realistic way. Then, a more accurate expression of the thermo-chemical efficiency can be written as:

$$\eta_{ch,new} = \frac{F_{0,CH_4} \cdot X \cdot \int_{T_0}^{T_{reactor}} Cp_{CH_4} \cdot dT + F_{0,CH_4} \cdot X \cdot \Delta H_1(T_{reactor}) + 1/2 \cdot F_{0,CH_4} \cdot X \cdot Y \cdot \Delta H_2(T_{reactor})}{P_{solar}} \quad (18)$$

and the thermal efficiency becomes:

$$\eta_{th,new} = \frac{F_{0,CH_4} \cdot \int_{T_0}^{T_{reactor}} Cp_{CH_4} \cdot dT + F_{0,CH_4} \cdot X \cdot \Delta H_1(T_{reactor}) + 1/2 \cdot F_{0,CH_4} \cdot X \cdot Y \cdot \Delta H_2(T_{reactor}) + F_{Ar} \cdot \int_{T_0}^{T_{reactor}} Cp_{Ar} \cdot dT}{P_{solar}} \quad (19)$$

For each run, the solar power is calculated from calorimetric measurements at the center of the reactor aperture. As a first approximation, the solar flux density is assumed homogeneous at the aperture, which may lead to a slightly over-estimated solar power. The net solar power absorbed varies between 16.9 kW and 25.8 kW depending on the working temperature between 1823 K and 2073 K. Fig. 11 illustrates the evolution of the above defined efficiencies at 1823 K, 1873 K, 1973 K, and 2073 K. For each temperature, the CH_4 mole fraction in the feed was 20%. Obviously, the thermo-chemical efficiency (Eq. 18) is always lower than the thermal efficiency (Eq. 19). The calculated reactor thermo-chemical efficiencies are improved when accounting for the presence of acetylene as a high energy value by-

product. In contrast, C_2H_2 formation lowers the power available for methane dissociation. Indeed, the amount of energy consumed per mole of converted methane is higher in the two-step endothermic and exothermic reaction scheme ($\Delta H_1 + \frac{1}{2} \cdot Y \cdot \Delta H_2$) than in the single-step CH_4 dissociation ($\Delta H_1 + \frac{1}{2} \cdot \Delta H_2$). Thus, the fraction of solar energy devoted to reaction enthalpy is strengthened when C_2H_2 intermediate is considered in the calculation.

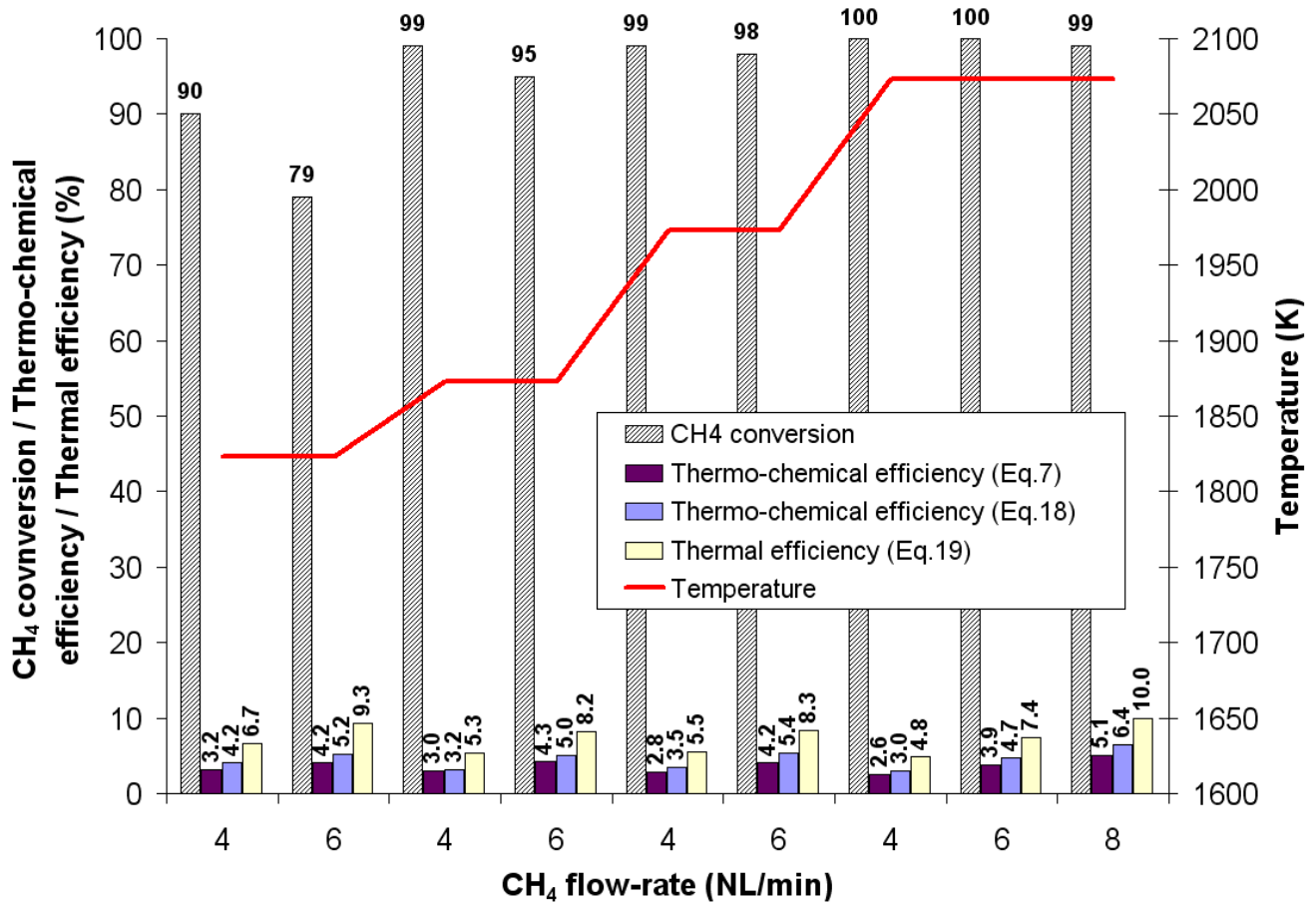


Figure 11. CH_4 conversion and reactor efficiencies (for a single-step reaction model or a two-step mechanism) as a function of temperature and CH_4 flow-rate (CH_4 mole fraction in the feed: 20%)

For a given temperature, an increase in CH_4 flow-rate results in significant efficiencies improvement (both thermo-chemical and thermal), but in counterpart it affects the CH_4 conversion, especially at low temperature. At 1823 K, CH_4 conversion is only 79% for 6 NL/min ($1 \times 10^{-4} \text{ Nm}^3 \text{ s}^{-1}$) of fed CH_4 , whereas CH_4 conversion is almost complete at higher temperatures. On the basis of the reported reactor

efficiencies, an optimum temperature for reactor operation may exist. Indeed, CH₄ conversion exceeds 95% for temperatures higher than 1873 K, while thermal efficiencies tend to decrease when increasing the temperature (9.3% at 1823 K and 7.4% at 2073 K for 6 NL/min (1×10^{-4} Nm³s⁻¹) of CH₄). This is due to the increased solar power input when raising the temperature, and to more induced radiation losses. In order to maximize both the CH₄ conversion and the thermal efficiency of the reactor, a temperature between 1873 K and 1973 K is advised, the smallest being preferable for coupling the process with existing solar concentrating technologies. The optimum temperature range has been identified on the basis of optimized reaction efficiencies. Further work is required to optimize as well the solar concentrating systems and the carbon black properties that are both key issues for the process economics. A 50 kW pilot-scale solar reactor is under construction to produce larger quantities of carbon black and to determine its properties. The main heat losses in the current solar reactor were identified to be infrared radiation emission through the window and conduction through the water-cooled front face. For increasing reactor efficiencies, the front face insulation should be improved and a higher solar concentration ratio is required to minimize IR-radiation losses.

4-Conclusion

Solar thermal dissociation of methane was investigated in a multi-tubular solar reactor prototype operating in the high temperature range 1823 K – 2073 K. A wide range of experimental conditions was tested: methane flow rate up to 12 NL/min (2×10^{-4} Nm³s⁻¹), CH₄ mole fraction in the feed up to 100%, and residence time from 10 ms and beyond 100 ms. CH₄ conversion chiefly increased with temperature and residence time, whereas C₂H₂ content in the off-gas was more lowered when raising the residence time than the temperature. C and H mass balances showed that C₂H₂ formation strongly alleviates the C yield. Moreover, a two-step reaction mechanism was proposed involving C₂H₂ intermediate. The highly endothermic C₂H₂ formation lowers the power available for methane dissociation. Both thermal and thermo-chemical efficiencies are improved when increasing the methane flow-rate in the feed. The

lower the temperature, the longer the required residence time for reducing C_2H_2 formation. A temperature of about 1873 K is advised to optimize both the methane conversion and the reactor thermal efficiency. A test with a different feedstock composition (natural gas instead of methane) did not modify the reactor performances.

A 50 kW pilot solar reactor is currently under construction to investigate the process at a larger scale, and to characterize the properties of the solar-produced carbon black with respect to the commercial standards.

Acknowledgements:

This work was financially supported by the European Project Solhycarb (2006-2010, Contract SES-CT2006-19770). Authors thank Jean-Louis Sans, Olivier Prévost, Marc Garrabos and Emmanuel Guillot for their technical support during the solar reactor manufacturing and the experimental campaigns at the 1 MW solar furnace of CNRS-PROMES (France).

Nomenclature:

C_{pi} specific heat of species i (J/mol.K, function of temperature)

E_a activation energy (J/mol)

F total molar flow-rate (mol/s)

F_i molar flow-rate of species i (mol/s)

$F_{0,i}$ inlet molar flow-rate of species i (mol/s)

ΔH° standard reaction enthalpy (J/mol)

k_0 pre-exponential factor (s^{-1})

m_i mass of species i (kg)

M_i molecular weight of species i (kg/mol)

NL Normal Liter (at normal conditions: 101.325 kPa and 273.15 K)

P absolute pressure (Pa)

P_{solar} solar power input (W)

Q_0 volumetric inlet flow-rate of argon and methane at the actual tube temperature and pressure (m^3/s)

R universal gas constant (8.314 J/mol K)

T absolute temperature (K)

T_0 reference temperature (298 K)

V_r volume of the isothermal part of the tubes where the reaction occurs (m^3)

X_{CH_4} methane conversion

Y_{C} carbon yield

Y_{H_2} hydrogen yield

y_i mole fraction of species i

Greek letters

τ space time (s)

τ_m mean residence time (s)

References:

- (1) DOE (Department of Energy). A multi-year plan for the hydrogen R&D program. Rationale, structure and technology roadmaps. Office of Power Delivery and Office of Power Technologies, 1999.
- (2) Dahl, J.K.; Buechler, K.J.; Finley, R.; Stanislaus, T.; Weimer, A.W.; Lewandowski, A.; Bingham, C.; Smeets, A.; Schneider, A. *Energy* 2004, 29(5-6), 715-725.
- (3) Donnet, J.B.; Bansal, R.C.; Wang, M.J.; *Carbon Black*, Second Edition, New York: Marcel Dekker, 1993.
- (4) Wyss, J.; Martinek, J.; Kerins, M.; Dahl, J.K.; Weimer, A.; Lewandowski, A.; Bingham C. *Int. J. Chem. Reactor Eng.* 2007, 5(A69).
- (5) Hirsch, D.; Epstein, M.; Steinfeld, A. *Int. J. Hydrogen Energy* 2001, 26(10), 1023-1033.
- (6) Holmen, A.; Olsvik, O.; Rokstad, O.A. *Fuel Process. Technol.* 1995, 42(2-3), 249-267.
- (7) Back, M.H.; Back, R.A. *Pyrolysis: theory and industrial practice*; New York: Academic Press, 1983, 1-24.
- (8) Jr. Gardiner, W.C.; Owen, J.H.; Clark, T.C.; Dove, J.E.; Bauer, S.H.; Miller, J.A.; McLean, W.J. *Syp. (Int.) Combust.* 1974, 15, 957.
- (9) Chen, C.J.; Back, M.H.; Back R.A. *Can. J. Chem.* 1975, 53, 3580-3590.
- (10) Lee, K.L.; Lee, S.Y.; Han G.Y., Lee B.K., Lee T.J., Jun J.H., Yoon K.J. *Carbon* 2004, 42, 2641-2648.
- (11) Muradov, N.; Smith, F.; T-Raissi, A. *Catal. Today* 2005, 102, 225-233.
- (12) Lédé, J.; Weber, C.; Villermaux, J. *Academie des Sciences (Paris), Comptes Rendus, Serie B - Sciences Physiques* 1978, 286(22), 299-302.
- (13) Billaud, F.; Baronnet, F.; Freund, E.; Busson, C.; Weill, J. *Rev. Inst. Fr. Pét.* 1989, 44(6), 813-823.

- (14) Steinfeld, A.; Kirillov, V.; Kuvshinov, G., Mogilnykh Y.; Reller, Chem. Eng. Sci. 1997, 52(20), 3599-3603.
- (15) Kogan, M.; Kogan, A. Int. J. Hydrogen Energy 2003, 28(11), 1187-1198.
- (16) Trommer, D.; Hirsch, D.; Steinfeld, A. Int. J. Hydrogen Energy 2004, 29(6), 627-633.
- (17) Kogan, A.; Kogan, M.; Barak, S. Int. J. Hydrogen Energy 2004, 29(12), 1227-1236.
- (18) Hirsch, D.; Steinfeld, A. Int. J. Hydrogen Energy 2004, 29(1), 47-55.
- (19) Abanades, S.; Flamant, G. Chem. Eng. Process.: Process Intensif. 2008, 47(3), 490-498.
- (20) Dahl, J.K.; Buechler, K.J.; Weimer, A.W.; Lewandowski, A.; Bingham, C. Int. J. Hydrogen Energy 2004, 29(7), 725-736.
- (21) Rodat, S.; Abanades, S.; Coulié, J.; Flamant, G. Chem. Eng. J., 2009, 146(1), 120-127.
- (22) Abanades, S., Flamant, G. Chem. Eng. Commun 2008., 195(9), 1159-1175.
- (23) Bruce Nauman, E. Ind. Eng. Chem. Res. 2008, 47, 3752-3766.
- (24) Happel, J.; Kramer, L. Ind. Eng. Chem. 1967, 59(1), 39-71.
- (25) Choudhary, T.V.; Aksoylu, E.; Goodman, D.W. Catal. Rev. 2003, 45(1), 151-203.
- (26) Olsvik, O; Rokstad, O.A.; Holmen; A. Chem. Eng. Technol. 1995, 18, 349-58.
- (27) Billaud, F.; Guéret, G.; Weill, J. Thermochim Acta 1992, 211, 303-322.
- (28) Fincke, J.R.; Anderson, R.P.; Hyde, T.A.; Detering, B.A. Ind. Eng. Chem. Res. 2002, 41(6), 1425-1435.